ACS APPLIED MATERIALS & INTERFACES

Research Article

www.acsami.org

Orientated Guidance of Peripheral Nerve Regeneration Using Conduits with a Microtube Array Sheet (MTAS)

Yueming Wang,[†,#] Wenjin Wang,[†,‡,#] Yan Wo,[†] Ting Gui,[†] Hao Zhu,[†] Xiumei Mo,[§] Chien-Chung Chen,[∇] Qingfeng Li,*[,‡] and Wenlong Ding*[,†]

[†]Department of Anatomy, Histology and Embryology, Shanghai Jiao Tong University School of Medicine, Shanghai, 200025, China

[‡]Department of Plastic and Reconstructive Surgery, Shanghai Ninth Hospital, Shanghai, 200011, China

[§]College of Chemistry, Chemical Engineering and Biotechnology, Donghua University, Shanghai 201620, China

[∇]Graduate Institute of Biomedical Materials and Tissue Engineering, Taipei Medical University, Taipei 11031, Taiwan

ABSTRACT: Material surface topography has been shown to affect the biological behavior of cells *in vitro*; however, the *in vivo* effect on peripheral nerve regeneration has not been explored. Here, we studied the potential of a microtube array sheet (MTAS) with a unique longitudinal surface topography to promote peripheral nerve regeneration efficiency, both *in vivo* and *in vitro*. Schwann cells, spinal cord motor neurons, and dorsal root ganglion neurons were seeded on the MTAS to study the effect of the construct on the biological properties and behaviors of neural cells. The MTAS guided the oriented migration of Schwann cells without affecting other critical biological properties, such as proliferation and neurotrophin expression. In addition, the MTAS guided the directed extension of neurites from both types of neurons. Next, we tested the capability of the MTAS to facilitate peripheral nerve regeneration by bridging a 10 mm sciatic nerve defect in rats with a nerve conduit equipped with an MTAS lining. The MTAS significantly promoted peripheral nerve regeneration, as suggested by the greater fiber caliber in the midconduit and the greater abundance of fibers in nerve segment distal to the conduit. Moreover, scanning electron microscopy (SEM) analysis suggested the orientated guidance of nerve regeneration by the MTAS, as indicated by the smaller eccentricity of the nerve fibers and the concordant arrangement of the collagen fiber in both the fibers and the matrix in the MTAS group. Our results collectively suggest that the conduits with the MTAS developed in this study have significant potential for facilitating peripheral nerve regeneration by modifying critical biological behaviors and guiding orientated nerve growth.

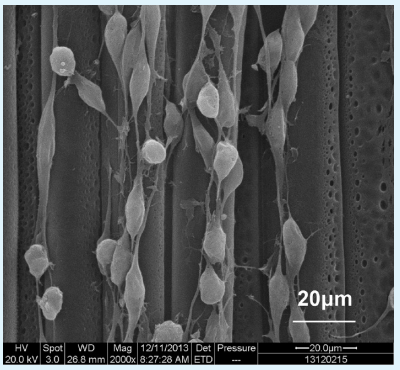

KEYWORDS: *nerve regeneration, nerve guide, surface topography, biomaterial, orientated nerve growth*

1. INTRODUCTION

Peripheral nerve injury is generally caused by trauma or tumors and the consequent surgery, resulting in a compromised quality of life, manifested by dysfunctional limbs or a distorted facial expression, which cause both physical and mental suffering. Although minor injuries, such as crushing, transection, or short nerve defects, can be repaired through delicate surgery, the regeneration of large nerve defects remains a major challenge, because of poor functional recovery, despite the regenerative capability of peripheral nerves and advances in microsurgery techniques. Autologous grafting is regarded as the gold standard for the repair of peripheral nerve defects, but its clinical application is limited due to the restricted supply of donor nerves and secondary injury at the donor site. The use of allografts and xenologous nerve grafts is accompanied by a risk of disease transmission and subsequent complications due to the use of immunosuppressants.[1] Biological materials, such as vessels, tendons, or muscles, despite their easy accessibility and biological compatibility, also hold several disadvantages, such as their susceptibility to collapse, scar formation, and secondary donor site injury.[2−4]

Synthetic nerve conduits are promising substitutes for autologous nerve grafting. These conduits are biocompatible, biodegradable, and mechanically strong enough to maintain the original shape and space for nerve regeneration. However, despite the encouraging morphological outcomes after conduit repair, further improvement is needed in functional recovery.[5] To achieve successful regeneration, several issues must be resolved, such as the mechanical properties, inner structure, electrical conductivity, and surface topography of the conduit.[6] Various efforts have been undertaken to improve these properties. Fibrous or spongy inner structures have been designed to guide nerve growth through the conduit.[7,8] For example, Xu and colleagues refined the conductivity of nerve conduits to facilitate nerve regeneration.[9] In recent years, surface topography has become a new focus of research interest in the field of tissue engineering. Human tissues are highly organized, with polarized cells arranged in a specific manner.

Received: November 15, 2014
Accepted: April 8, 2015
Published: April 8, 2015

DOI: 10.1021/acsami.5b00215
ACS Appl. Mater. Interfaces 2015, 7, 8437−8450

Neural cells are one of the most notable examples of a highly polarized cell type, typically extending one or several neurites to connect to specific targets in the body. When bridging nerve defects with nerve conduits, the surface of the conduit or the inner structure interacts directly with the regenerating axons or Schwann cells. Moreover, the biological properties and behaviors of cells may be modified or regulated by the surface geometry of the interacting biomaterials. Tay and colleagues reported that, upon culture on 20-μm micropatterned wide adhesive strips, human mesenchymal stem cells exhibit elongated morphology and upregulation of hallmark genes involved in neurogenesis and myogenesis.[10] The improvement of nerve regeneration efficiency via the design of proper surface geometry is critical, as faster regeneration rescues degenerated muscle fibers and improves functional recovery. The micropatterned surface geometry mimics well-organized tissue structures, such as tendon and nerves, and has been explored for its potential use in rebuilding musculotendinous organs or nerves.[11] Béduer et al.[12] reported that micropatterned surfaces induce the differentiation of adult human neural stem cells and guide the regular alignment of neurites along the edges of the microchannels. These authors further determined that a 20-μm width is optimal for directed neurite extension without compromising the growth rate. Studies on peripheral glial cells by Miller et al.[13] revealed similar behavioral changes in Schwann cells with surprisingly concordant data, suggesting that the micropatterned groove width affects Schwann cell orientation (10−20 μm being the optimal width) and that the speed and direction of neurite extension are also affected by the surface topography.[14] Therefore, by modifying the biological behaviors of neural cells, micropatterned biomaterials have great potential to facilitate nerve regeneration.

The currently used conduits are either woven, molded, or electrospun nerve guides,[15−17] with the conduit wall comprising a lattice of interwoven or concentrically aligned fibers in the inner surface. Instead of being parallel to the direction of nerve growth, these fibers are aligned in transverse, oblique, or even randomly dispersed patterns that might compromise the efficiency of regeneration.

Electrospinning represents a versatile, low-cost method to produce microscale to nanoscale fibrous membranes. The most up-to-date technique has led to the generation of a novel monolayer sheet with a highly aligned structure that mimics tissue structures for improved regeneration.[18−20] Using this technique, large pieces of microtube array sheet (MTAS) are prepared as single-layered hollow fibrous assemblies with an extremely high degree of fiber alignment. The MTAS has a unique surface geometry with longitudinally aligned parallel grooves similar to the previously reported micropatterned membrane.[21−24] The purpose of the current study was to explore the potential of an MTAS with a unique surface topography to promote peripheral nerve regeneration, both *in vitro* and *in vivo*. The biocompatibility and cytotoxicity of the sheet were tested using a series of cell growth analyses, and its effects on the biological properties and behavior of neural cells were examined via co-culture with Schwann cells, dorsal root ganglia, and spinal motor neurons. For *in vivo* analyses, the MTAS was used as a lining of the conduit to bridge a 10 mm sciatic nerve defect in rats and its capability to promote peripheral nerve regeneration was assessed.

2. MATERIALS AND METHODS

2.1. Preparation of Microtube Array Sheet (MTAS) and Conduits. The preparation of poly-L-lactic acid (PLLA) MTAS was described previously.[21−24] The materials used were (1) PLLA (medical grade, Mw = 140 kDa; BioTechOne, Inc., Taiwan), (2) polyethylene glycol/poly(ethylene oxide) (PEG, Mw = 36 kDa; PEO, Mw = 900 kDa; both from Sigma−Aldrich, USA), (3) *N*,*N*-dimethylformamide (DMF, $HCON(CH_3)_2$, 99.8%; Tedia, USA), and (4) dichloromethane (DCM, CH_2Cl_2, reagent grade, 99.9%; Mallinckrodt, USA). The following electrospinning dopes were prepared: (a) PLLA dissolved in a mixed DCM/DMF (8:2 vol %) solvent at room temperature to prepare a 15 wt % solution (shell) and (b) an aqueous solution of PEO/PEG (1:1) 10 wt % (core). An electrostatic charger (Charge-Master, Simco-Ion, Alameda, CA, USA) or a high-voltage power supply unit (You-Shang Co., FongShan City, Taiwan) was used as the electrostatic source. Typically, the electrospinning process was carried out by delivering the PLLA (shell) and PEG (core) solutions through a house-made coaxial spinneret with a syringe pump (KDS-100, KD Scientific, Holliston, MA, USA) at a rate of 4−9 mL/h, along with 5−7 kV of applied voltage and 3−5 cm of distance to a rotating drum collector. All electrospinning was carried out in a chamber under a relative humidity of 50% ± 5% and 25 ± 1 °C. PLLA MTAS was obtained by washing to remove the core component of PEG, followed by drying. Preconditioned medium was obtained by soaking the MTAS in culture medium at 37 °C for 48 h. For the animal experiments and cellular assays, the sheet was cut into 1-cm-long sections and placed as a lining within 14-mm-long conduits.

The conduits were a kind gift from Professor Mo Xiumei and were prepared as previously described. Briefly, raw silk was degummed three times with 0.5% (w/w) Na_2CO_3 solution at 100 °C for 30 min each and then washed with distilled water. The degummed silk was dissolved in a ternary solvent system composed of a $CaCl_2/H_2O$/EtOH solution (molar ratio of 1/8/2) for 1 h at 70 °C. After dialysis with a cellulose tubular membrane (250-7u; Sigma) in distilled water for 3 days at room temperature, the SF solution was filtered and lyophilized to obtain the regenerated SF sponges.

Pure SF, SF/P(LLA-CL) blends with different weight ratios and pure P(LLA-CL) were dissolved in HFIP solvents and stirred at room temperature for 6 h. The SF/P(LLA-CL)(50:50) blends were dissolved in HFIP solvent to prepare solutions with different concentrations from 4 to 12 w/v%. The solutions were filled into a 2.5 mL plastic syringe with a blunt-ended needle. The syringe was placed in a syringe pump (No. 789100C, Cole-Parmer, USA), and the solutions were dispensed at a rate of 1.2 mL/h. A voltage of 12 kV was applied using a high-voltage power supply (Model BGG6-358, BMEICO, China) across the needle and ground collector, which was placed at a distance of 12−15 cm.

2.2. Animals. Twelve adult female Sprague−Dawley rats (200−220 g) from the Animal Care Facility of Shanghai Jiao Tong University School of Medicine (Shanghai, China) were used for the experiments. All surgical procedures were performed under aseptic conditions on animals that were deeply anesthetized with sodium pentobarbital (40 mg/kg body weight). The experiments were carried out under the guidelines of the Chinese Council for Animal Care, approved by the Animal Care Committee of the Laboratory Animal at Shanghai Jiao Tong University School of Medicine.

2.3. Sciatic Nerve Surgery. For the sciatic nerve study, rats were randomly divided into control and experimental groups (6 rats in each group). The sciatic nerves were repaired either solely with a 14 mm-long nerve conduit or with a conduit with an MTAS lining using four stitches of 9−0 microsutures (Jin Huan Co.) through the epineurium on each end under 20−40× magnification following the removal of a 1 cm length of nerve from the midthigh. The rats were sacrificed 8 weeks later. The animals were deeply anesthetized before being perfused through the left ventricle. A warm saline flush (150 mL) was followed by 500 mL 4% paraformaldehyde in 0.1 M Sorensen's phosphate buffer. The nerve distal to the conduit and the gastrocnemius muscle were harvested for later immunostaining.

DOI: 10.1021/acsami.5b00215
ACS Appl. Mater. Interfaces 2015, 7, 8437−8450

2.4. Primary Cultures of Schwann Cells. Schwann cell cultures were obtained using the method of Brockes et al.,[25] with minor modifications. Briefly, the sciatic nerves and brachial plexus from 2−3-day-old Sprague−Dawley rats were harvested and digested with 0.12% collagenase and 0.05% trypsin (Sigma) at 37 °C for 15 min. At 24 h after plating, the cells were treated with cytosine arabinoside (5 μg/mL; Sigma) for 3 days to eliminate proliferating fibroblasts. Following treatment, the culture medium was replaced with fresh medium supplemented with forskolin (2 μM; Sigma) and basic fibroblast growth factor (bFGF; 20 ng/mL; R&D Systems, Minneapolis, MN, USA) to facilitate Schwann cell proliferation. After 8 days, the Schwann cells were detached with 0.125% EDTA-trypsin (Sigma) and passaged. The culture medium was changed three times per week. The cells were treated with preconditioned medium or seeded on the MTAS after the second passage.

2.5. Dorsal Root Ganglion (DRG) Neuron Cultures. Primary cultures of DRG neurons were prepared from embryonic day 14 (E14) Sprague−Dawley rats. The DRG neurons were dissected in D-Hank's buffered salt solution, followed by incubation in 0.05% trypsin at 37 °C for 15 min. The reaction was terminated by adding DMEM with 10% fetal calf serum, and the cells were triturated 40−60 times using a fire-polished Pasteur pipet. The neurons were resuspended in neurobasal medium supplemented with 2% B27 and 1 mM L-glutamine following centrifugation at 1500 rpm for 5 min. Next, the neurons were seeded at a density of 1×10^6 cells/mL onto poly-L-lysine-coated Petri dishes or an MTAS and cultured at 37 °C in a humidified atmosphere with 5% CO_2. The medium was replaced every 3 days.

2.6. Spinal Cord Motor Neuron Culture. The spinal cords were harvested from E12 rat embryos and incubated in 2 mL 0.05% trypsin and 0.12% collagen (Invitrogen) in L15 for 15 min at 37 °C. The cells were harvested by centrifugation at 1500 rpm for 5 min and resuspended in neurobasal medium. Motor neurons were purified via gradient centrifugation using NycoPrep (NycoPrep A 1.077, Axis-Shield, Norton, MA). An aliquot (3 mL) of the cell suspension was layered onto NycoPrep discontinuous density gradients containing 2 mL of 8.01% solution of Nycodenz (*N*,*N*′-bis(2,3-dihydroxypropyl)−5-[*N*-(2,3-dihydroxypropyl) acetamido]−2,4,6-triiodo-isophthalamide), 2 mL of 7.66% solution, and 2 mL of 7.05% solution after centrifugation at 500*g* for 20 min at 4 °C. The motor neurons were collected as a white turbid band at the interface of the medium and the 7.05% solution. To harvest motor neurons, the top layer of each gradient, consisting of the medium, was carefully removed. The band of motor neurons from the first interface of each gradient was aspirated and pooled into a new 15 mL centrifuge tube. Next, the motor neurons were washed with 0.004% DNase-containing medium and centrifuged at 300*g* for 10 min at 4 °C. The cells were resuspended in neurobasal medium supplemented with B27 and seeded at a density of 10^6 live cells/mL in six-well plates or onto MTAS precoated with poly-L-lysine (PLL, Sigma) and placed in a 5% CO_2 incubator at 37 °C.

2.7. MTT Assay. The MTT (3(4,5-dimethylthiazol-2-yl)2,5-diphenyltetrazolium bromide) assay was used to study the effect of the MTAS on Schwann cell growth. Cells in a 96-well plate were treated with complete medium and material-preconditioned medium for 12, 24, 36, 48, 60, 72, 96, and 120 h. The MTT stock solution (10 mL of 10 mg/mL, Sigma) was added to the remaining medium, and the cultures were incubated for an additional 4 h at 37 °C. The medium was discarded after incubation, and the insoluble dark blue formazan was dissolved in 100 μL DMSO and quantified at 570 nm with a reference wavelength of 630 nm, using a microtiter plate reader (Bio-Tek Inc., USA). The survival of the positive control group was defined as 100%, and that of treated groups was expressed as a percentage of the positive control value.

2.8. BrdU Analysis. Schwann cell proliferation was analyzed using a colorimetric BrdU cell proliferation ELISA kit (Roche Applied Science, Mannheim, Germany). Schwann cells were resuspended in complete or material-preconditioned medium, plated at a density of 5×10^4 cells/mL (200 μL per well) on 0.01% poly-L-lysine-coated 96-well plates, and incubated at 37 °C with 5% CO_2 for 48 h. BrdU was added at the indicated time-points, followed by incubation for 2 h. The proliferation assay was carried out according to the manufacturer's protocol. The reaction products were quantified by measuring the absorbance at 370 nm (reference wavelength, 492 nm) using a scanning multiwell spectrophotometer equipped with Gen 5 analysis software (Synergy HT multimode microplate reader, BioTek Instruments Inc., Bad Friedrichshall Germany). The absorbance results were directly correlated with the amount of DNA synthesis and thus the number of proliferating cells. The assays were performed three times using triplicate wells.

2.9. Transwell Analysis. Schwann cell migration was evaluated using 6.5 mm Transwell chambers with 8 μm pores (Costar, Cambridge, MA), as described previously.[26] The bottom surface of each membrane was coated with 10 μg/mL fibronectin. The Schwann cells were resuspended in 100 μL DMEM. Preconditioned DMEM was transferred to the top chambers of each transwell at a density of 10^6 cells/mL, and 600 μL of complete medium was injected into the lower chambers. The cells were allowed to migrate at 37 °C, 5% CO_2 for 6 h before fixation with 4% phosphate-buffered paraformaldehyde. The upper surface of each membrane was cleaned with a cotton swab. The cells adhering to the bottom surface of each membrane were stained with 1% eosin and imaged under a microscope (Leica DM4000 B, Leica Microsystems, Germany). Cells from three random fields were counted for each of the triplicate wells.

2.10. Real-time PCR. Total RNA was isolated with TRIzol reagent (Invitrogen, USA) according to the manufacturer's instructions, and the recovery was measured based on absorbance at 260 and 280 nm. Total RNA samples (2 μg) were further reverse-transcribed with the PrimeScript RT Reagent Kit (Perfect Real Time, TaKaRa Biotechnology, Japan) using the manufacturer's protocol. The mRNA levels of brain-derived neurotrophic factor (BDNF), ciliary neurotrophic factor (CNTF), glial cell line-derived neurotrophic factor (GDNF), nerve growth factor (NGF) and Neurotrophin-4 (NT4) were quantitatively measured using the Applied Biosystems step-one plus Real-Time PCR System (Life Technologies, USA) using SYBR Select Master Mix (Life Technologies, USA). Glyceraldehyde 3-phosphate dehydrogenase (GAPDH) was used as the nonregulated control for the normalization of BDNF, CNTF, GDNF, NGF, and NT_4 mRNA expression. The sequences of the forward and reverse primers are listed in Table 1. The threshold cycle (Ct) was calculated using the second-derivative maximum method. The data were analyzed via the delta−delta method. The assays were performed three times using triplicate wells. The final values are expressed as the ratio versus the control.

Table 1. Primer Sequences for Real-Time PCR

primer	sequence
GAPDH −F	AGGGTGGTGGACCTCATGG
GAPDH −R	AGCAACTGAGGGCCTCTCTCTT
NGF-F	GTCTGGGCCCAATAAAGGCT
NGF-R	CTGTGTACGGTTCTGCCTGT
NT4-F	TTGACAGGTGTGCAAAGCCAT
NT4-R	GGAGACAAGAGGTCCCACTC
CNTF-F	GAGAACCTCCAGGCTTACCG
CNTF-R	CTAGCTGGTAGGCAAAGGCA
GDNF-F	CACCAGATAAACAAGCGGCG
GDNF-R	TCGTAGCCCAAACCCAAGTC
BDNF-F	GTCACAGCGGCAGATAAAAAG
BDNF-R	ATGGGATTACACTTGGTCTCGT

2.11. Electron Microscopy. Scanning electron microscopy (SEM) (Model Quanta-200, Philips-FEI, EIndhoven, The Netherlands) was used to characterize the morphology of the cell-to-cell and cell-to-material contacts. The material was cut into 1 cm × 1 cm sections and seeded with Schwann cells (1×10^6 cells/mL) at 40 μL per piece in 24-well plates. The cells were fixed for 24 h with 2.5% glutaraldehyde (pH 7.4) at 2−3 days after seeding, followed by treatment with 1% osmium tetroxide for 4 h. The constructs were

DOI: 10.1021/acsami.5b00215
ACS Appl. Mater. Interfaces 2015, 7, 8437−8450

dehydrated in a graded series of ethanol for 10 min, critically point-dried, and sputtered with gold.

Ultrathin sections of regenerated nerve tissues were stained with lead citrate and uranyl acetate and examined via transmission electron microscopy (TEM) (Model JEM-1200 EX, JEOL, Japan).

2.12. Flow Cytometry. Schwann cell apoptosis was assessed using an Annexin V-FITC/PI apoptosis detection kit (BD Biosciences Clontech, USA). Schwann cells were resuspended in complete and preconditioned medium and plated at a density of 1×10^6 cells/mL at 1 mL per well on 0.01% poly-L-lysine-coated six-well plates. The cells were incubated at 37 °C, 5% CO_2, for 48 h and trypsinized with a 0.125% trypsin-EDTA solution. All subsequent staining was performed following the manufacturer's instructions. Apoptotic and necrotic cells were distinguished on the basis of annexin V-FITC reactivity and PI exclusion. The samples were washed twice and adjusted to a concentration of 1×10^6 cells/mL with PBS at 4 °C. Next, 100 μL of the suspension was added to each labeled tube, and 10 μL of Annexin V-FITC and 10 μL of 20 μg/mL PI were added to the labeled tube and incubated for at least 20 min at room temperature in darkness. PBS binding buffer (400 μL) was added to each tube without washing, followed by rapid analysis within 30 min using the FACSCalibur flow cytometer (Becton Dickinson, USA).

2.13. Immunostaining. For immunocytometry, cell cultures were fixed with 4% PFA for 20 min at room temperature, washed three times for 5 min in 0.01 M phosphate-buffered saline (PBS), blocked with 10% normal goat serum (NGS) for 1 h at RT, and incubated with primary antibodies overnight at 4 °C. After three 10 min washes in PBS, the cultures were incubated with secondary antibodies for 1 h at 37 °C and rinsed three times for 5 min in PBS, followed by 10 min incubation in Hoechst solution (Hoechst 33342, 1:5000; Invitrogen, USA) and another three washes in PBS. The coverslips were mounted with Gel/Mount aqueous mounting medium (Biomeda Corp.). The Schwann cells were stained with anti-S-100 (1:200, Abcam, USA), and the neurons and nerve fibers were stained with anti-β-tubulin (1:100, Sigma–Aldrich, USA). The secondary antibodies were conjugated to FITC or Cy3 (1:200, Abcam, USA). For immunohistochemistry, post-fixation of the nerve and muscle was performed in the same solution as that used for perfusion overnight, followed by immersion in 20% sucrose in 0.1 M Sorensen's phosphate buffer. Ten micrometer (10 μm) sections were cut on a freezing microtome (Thermo), mounted on glass slides and dried for future immunostaining. The slides were washed three times for 5 min in 0.01 M PBS, blocked with 10% NGS for 1 h at RT, and incubated with primary antibodies overnight at 4 °C (anti-β-tubulin for staining of nerve fibers in the distal nerve and PGP9.5 for the staining of nerve terminals in the muscle). After three 10 min washes in PBS, the slides were incubated with secondary antibodies for 1 h at 37 °C and rinsed three times for 5 min in PBS. To stain the end plate, the slides with muscle tissue were incubated with bungarotoxin at 37 °C for another 5 h, followed by three 10 min washes in PBS. The coverslips were mounted with Gel/Mount aqueous mounting medium (Biomeda Corp.) and observed under a light microscope.

2.14. Image Analysis. TEM images acquired at 2500× magnification were used to evaluate the nerve fiber diameter, G ratio, and eccentricity. Ten random visual fields were collected from each sample. The maximum and minimum fiber calibers (both with and without the myelin sheath) were measured with the Image Process Plus software (version 4.5) for each nerve fiber. Only myelinated fibers were counted. For fiber caliber comparison, the mean value of the fiber caliber of all fibers in each sample was calculated for later statistical analysis. For fiber caliber distribution analysis, the data from all 10 fields were summarized to calculate the distribution frequency for each sample. The G ratio was calculated as the ratio of the inner diameter to the outer diameter. The eccentricity rate was calculated using the following formula:

$$\text{eccentricity} = \sqrt{1 - \frac{b^2}{a^2}}$$

where a refers to the longest diameter and b refers to the shortest diameter. Axonal diameter and neural tissue area were measured with Image Process Plus (version 4.5).

The neural tissue areas were calculated with Image Process Plus (version 4.5). Only areas positively stained with tubulin were counted. For the counting and analysis of the nerve fibers in the distal nerve, images were acquired at 400× magnification and merged to produce an image of an intact nerve. The nerve fibers were counted manually. Five random visual fields at 10× magnification were selected for the gastrocnemius muscle sections, and 10 slides from each muscle were counted for the end-plate quantity in the reinnervated muscle. Only end-plates double stained by both bungarotoxin and PGP9.5 were counted.

2.15. Statistical Analysis. All numerical data are presented as the means ± standard deviation. Significant differences among the groups were analyzed via one-way analysis of variance (ANOVA), followed by Tukey's post-hoc test, using SPSS 14.0 software for Windows (student version). Significant differences between the median values were determined with a Mann–Whitney U test. Differences were statistically significant at $P < 0.05$.

3. RESULTS

3.1. Characterization of MTAS. As shown in Figure 1, the MTAS comprised assemblies of microtubes. The microtubes were aligned in parallel into a paper-thin sheet with a thickness

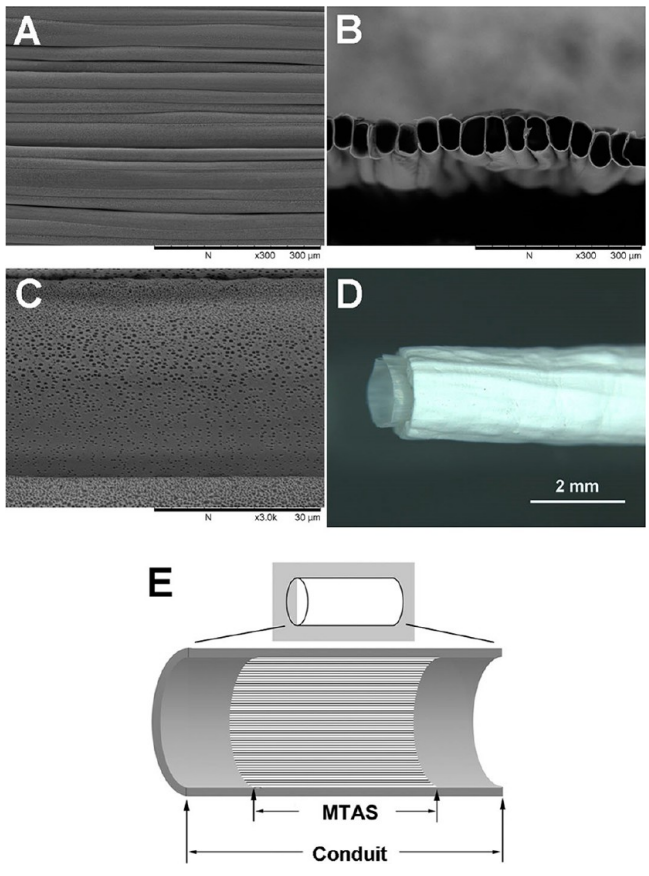

Figure 1. Surface geometry of the PLLA MTAS under scanning electronic microscopy (SEM). Longitudinally arranged, parallel V-shaped grooves were formed by the adjacent microtubes: (A) paralleled and longitudinal grooves could be found on the surface of the MTAS (scale bar = 300 μm), (B) transverse view of the MTAS, (C) pores are visible in the high-magnification view (scale bar = 30 μm), (D) construct of the conduit and the MTAS; the MTAS was pulled out of the conduit for better visualization, and (E) schematic view of the construct of the conduit and the MTAS.

DOI: 10.1021/acsami.5b00215
ACS Appl. Mater. Interfaces 2015, 7, 8437–8450

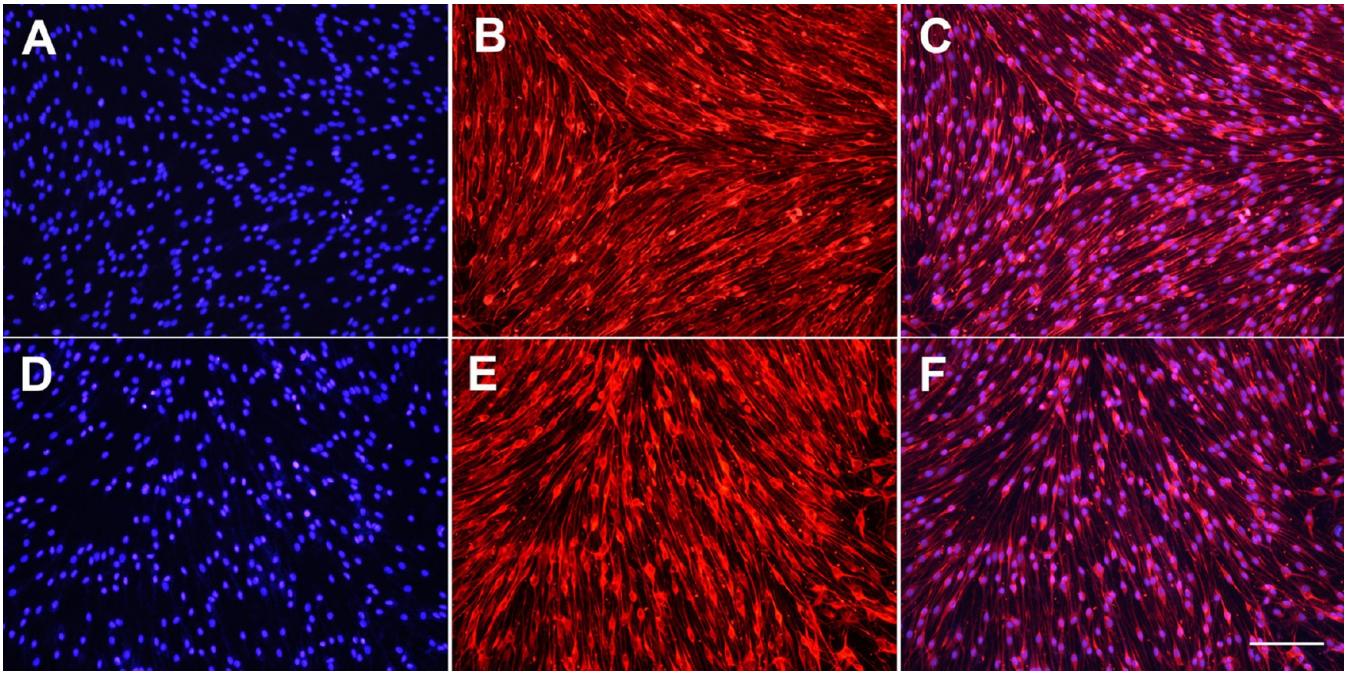

Figure 2. Schwann cell growth in a preconditioned medium. There were no morphological changes in the Schwann cells when they were cultured in a preconditioned medium pretreated with the MTAS at 37 °C for 48 h. The Schwann cells displayed an identical morphology in the both (A–C) control and (D–F) preconditioned medium samples. Panels A and D show Hoechst staining of all nuclei, panels B and E show S100 staining of Schwann cells, and panels C and F show merged images (200× magnification). Scale bar = 100 μm.

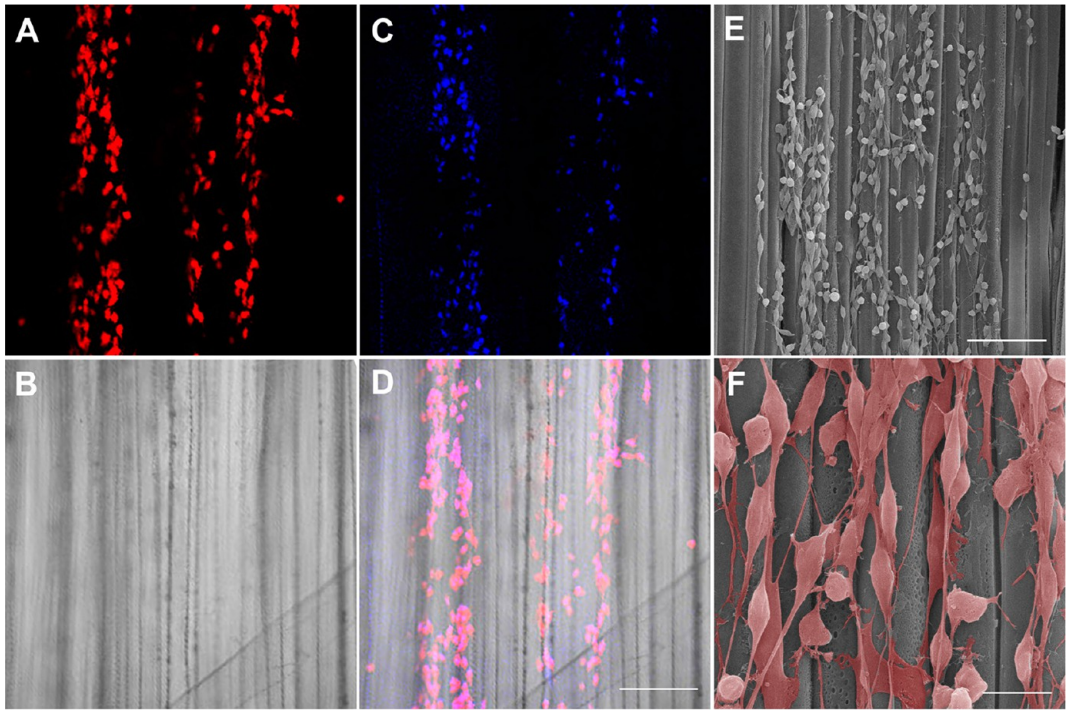

Figure 3. Schwann cell alignment on the MTAS: (A–D) confocal images ((A) S100 staining, (B) MTAS, (C) Hoechst staining, and (D) merged image; scale bar = 100 μm) and (E and F) SEM images ((E) scale bar = 100 μm, (F) 20 μm). A fundamental change in the pattern of cell alignment or distribution was noted when the Schwann cells were cultured directly on the MTAS. Both the SEM and immunostaining findings revealed that these Schwann cells were rearranged in a linear manner parallel to the grooves on the surface of the MTAS after 24 h of culture, despite the initial random seeding. The cells exhibited the typical healthy bipolar morphology on the MTAS, extending long processes and connecting with each other from both ends.

of 50 μm. Numerous parallel and longitudinally oriented grooves were formed between two adjacent microtubes, constituting a unique surface geometry. Each groove had a V shape in the transverse section. The average depth of the groove was 8 μm, and the average width was 20 μm, as measured from the transverse view with SEM (Figure 1). The

DOI: 10.1021/acsami.5b00215
ACS Appl. Mater. Interfaces 2015, 7, 8437–8450

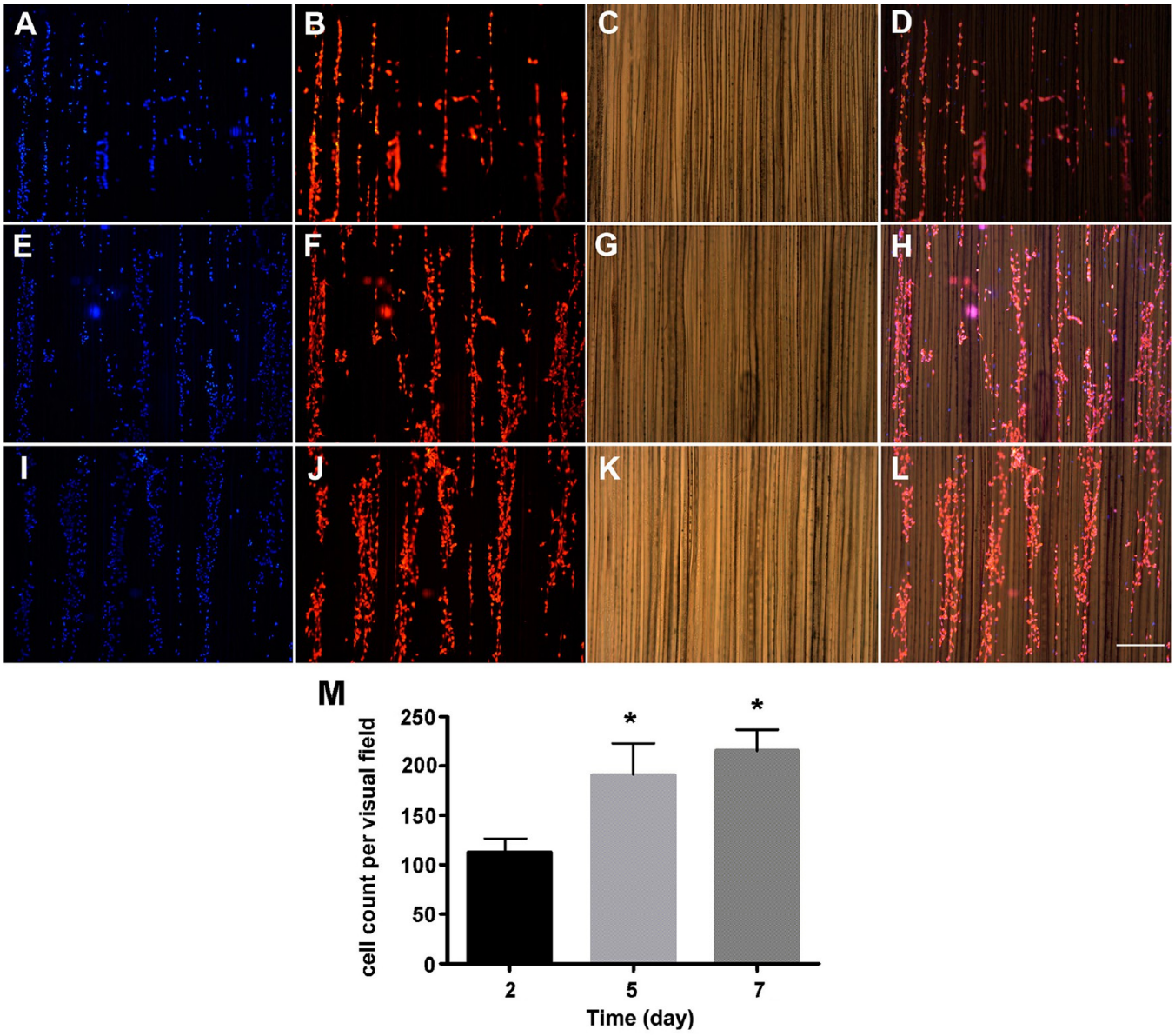

Figure 4. Schwann cell growth on the MTAS: (A–D) 2 days after plating, (E–H) 5 days after plating, and (I–L) 7 days after plating. (Panels A, E, and I show Hoechst staining of the nucleus; panels B, F, and J show S100 staining of Schwann cells; panels C, G, and K show MTAS (viewed with white light); and panels D, H, and L show merged images. Scale bar = 200 μm.) Panel M shows an obvious increase in cell number over time in the low-magnification view when the Schwann cells were cultured directly on the MTAS (asterisk (*) indicates $p < 0.05$ vs 2 d). The longitudinal alignment of the cells was consistent with time.

MTAS was placed in a nerve conduit with an inner diameter of 1.5 mm as a single-layered lining for the subsequent *in vivo* studies.

3.2. Effect of the MTAS on the Biological Behaviors of Primary Cultured Neural Cells. To determine the effect of MTAS on the behavior of neural cells, primary cultured Schwann cells, DRG neurons and spinal cord motor neurons were cultured either in preconditioned medium pretreated with MTAS at 37 °C for 48 h or directly on the MTAS. The Schwann cells displayed an identical morphology in both the preconditioned and control media and were distributed at large in a spiral manner (Figure 2). However, as indicated in Figure 3, a fundamental change in the pattern of cell alignment or distribution was evident when the Schwann cells were cultured directly on the MTAS. Both the SEM and immunostaining findings revealed that these Schwann cells were rearranged in a linear manner. parallel to the grooves on the surface of the MTAS after 24 h of culture, despite the initial random seeding. The cells in this group exhibited a healthy bipolar morphology, extending long processes and connecting with each other from both ends. Moreover, the cell number increased with the time of culture (Figure 4). Similar patterns of neurite extension were observed in the DRG neuron and spinal cord motor neuron cultures. The DRG neurons extended long processes along the grooves and formed synapses with other DRG neurons that were in the same longitudinal line. Axons extending from the neurons were mostly directed along and parallel to the grooves. Few, if any, transversely directed axons were found between the neurons, despite the closer proximity of the cell bodies, which were distinguishable from those cultured on the Petri dishes, where they extended neurites in all directions and preferred to synapse with the nearest neurons (Figure 5). A longitudinal

DOI: 10.1021/acsami.5b00215
ACS Appl. Mater. Interfaces 2015, 7, 8437–8450

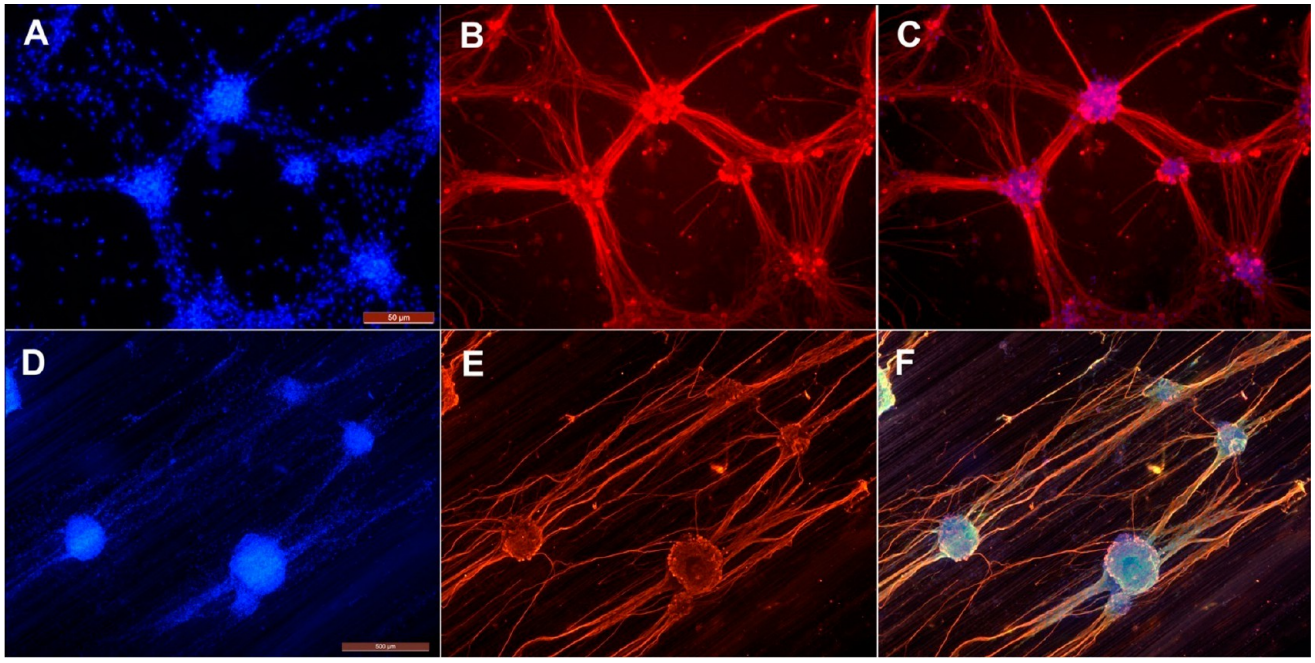

Figure 5. DRG explants co-cultured with MTAS. DRG neurons extended neurites in all directions when cultured on a Petri dish (panels A–C) and preferred to synapse with the nearest neurons. However, the pattern of neurite extension was greatly modified by the surface geometry of the MTAS, where the DRG neurons extended long processes along the grooves and formed synapses with other DRG neurons only in the same longitudinal line (panels D–F). Axons extending from the neurons were mostly directed along and parallel to the grooves. Few, if any, transversely directed axons were found between neurons, despite the closer proximity of cell bodies, which were distinguishable from those cultured on the Petri dishes. Panels A and D show Hoechst staining; panels B and E show Tubulin-III staining; and panels C and F show merged images.

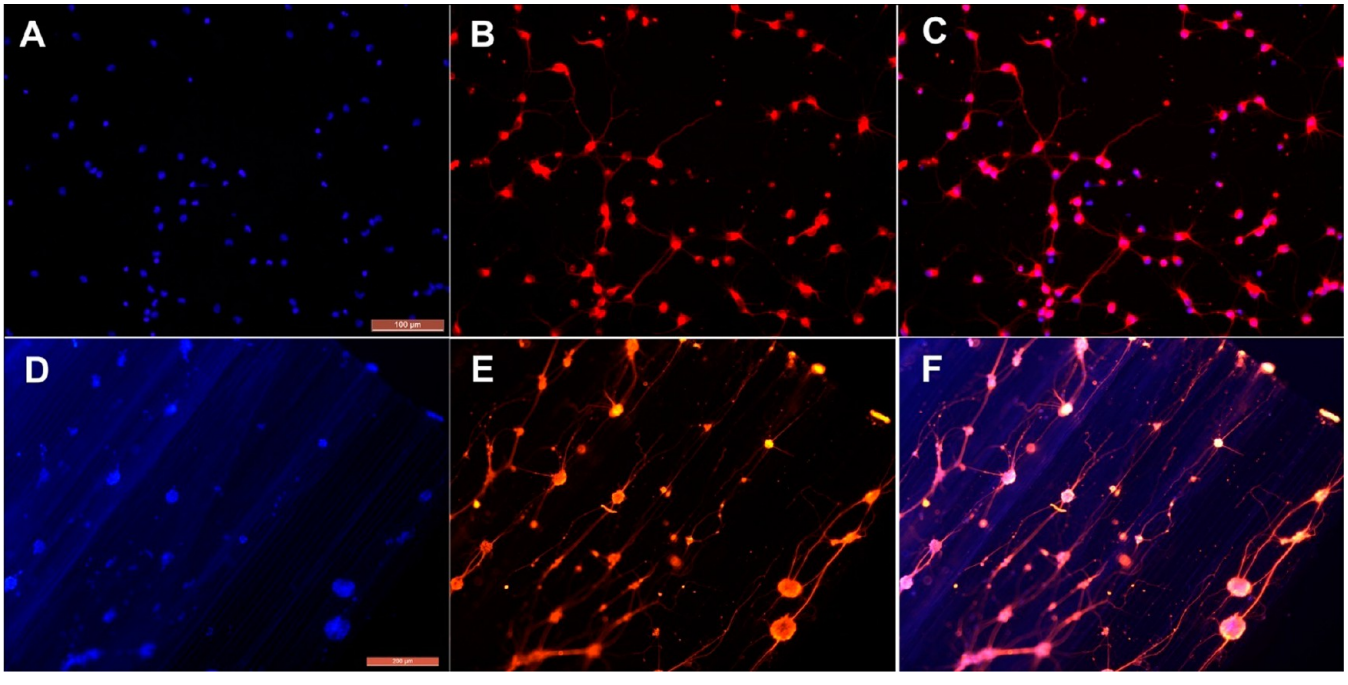

Figure 6. Spinal cord motor neuron co-cultured with an MTAS. The spinal cord neurons extended axons randomly when cultured on a Petri dish (panels A–C). However, the direction of neurite extension was modified when the cells were cultured on an MTAS, and the axons tended to grow along the grooves (panels D–F). Panels A and D show Hoechst staining, panels B and E show Tubulin-III staining, and panels C and F show merged images.

trend of neurite distribution that extended parallel to the grooves was also obvious in spinal cord neurons compared with their counterparts cultured on a Petri dish (Figure 6).

3.3. Toxicity and Biocompatibility of MTAS. To assess the toxicity and biocompatibility of MTAS, primary rat Schwann cells were cultured for 5 days following medium preconditioning by soaking the MTAS in the culture medium at 37 °C for 48 h. An MTT analysis was conducted at 12, 24, 36, 48, 60, 72, 96, and 120 h. The MTT data showed that the quantities of Schwann cells in both groups increased from 24 h

DOI: 10.1021/acsami.5b00215
ACS Appl. Mater. Interfaces 2015, 7, 8437–8450

and reached a plateau by 48 h (Figure 7). No significant differences were evident at each time-point, and treatment with

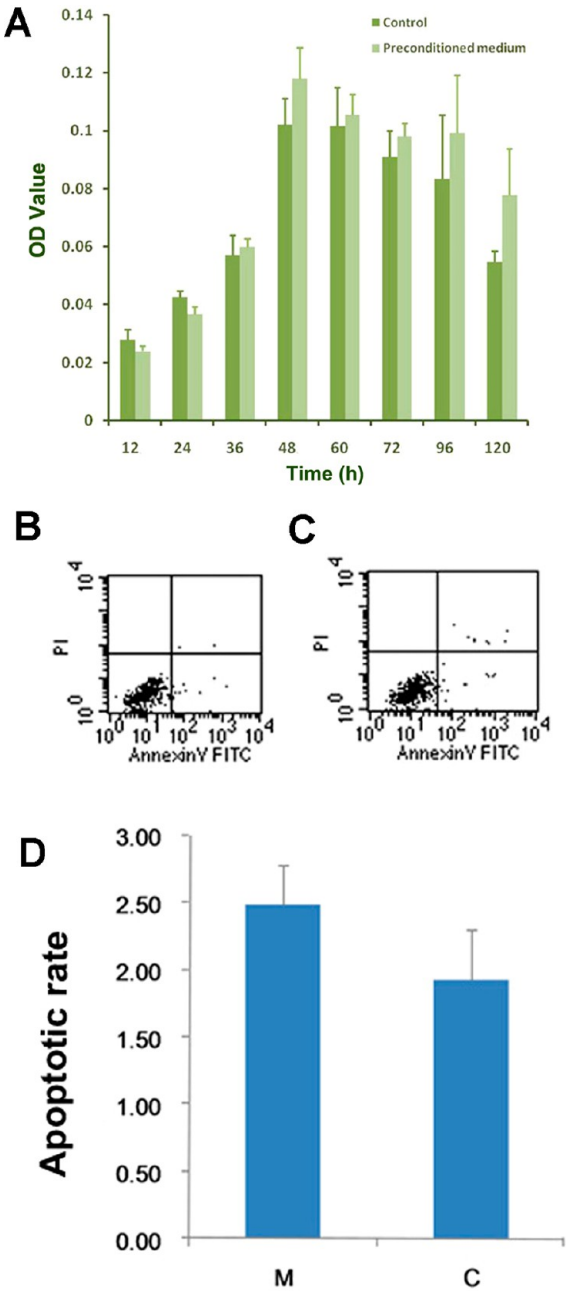

Figure 7. Effect of preconditioned medium on (A) the viability and (D) apoptotic rate of primary cultured Schwann cells: the preconditioned medium did not cause a significant change in the growth curve of primary Schwann cells, as indicated by the MTT assay. A slightly higher apoptotic rate was noted, but it was not statistically significant (panel B shows data for a cell cultured in an MTAS preconditioned medium, and panel C shows data for a cell cultured in the control medium). (In panel D, M denotes the MTAS-preconditioned group and C denotes the control group.)

preconditioned culture medium did not result in a left or right shift of the curve, suggesting that the cell growth was not affected by a preconditioned medium. Flow cytometry was further applied to examine the rate of cell apoptosis after a 2-day culture in a preconditioned medium. As indicated in Figure 7, exposure to a preconditioned medium did not lead to a significant increase in the apoptotic rate of cells.

3.4. Effect of MTAS on Cell Viability and Biological Properties. The biological activities of Schwann cells, including proliferation, migration, and neurotrophic factor production, which are critical for peripheral nerve regeneration, were evaluated following culture in a preconditioned medium. As indicated with BrdU analysis, no significant differences were observed between the control and preconditioned medium groups after a 2-day treatment period (Figure 8). Similarly, a transwell analysis to assess the cell migration capacity revealed no significant differences between the two groups (Figure 8).

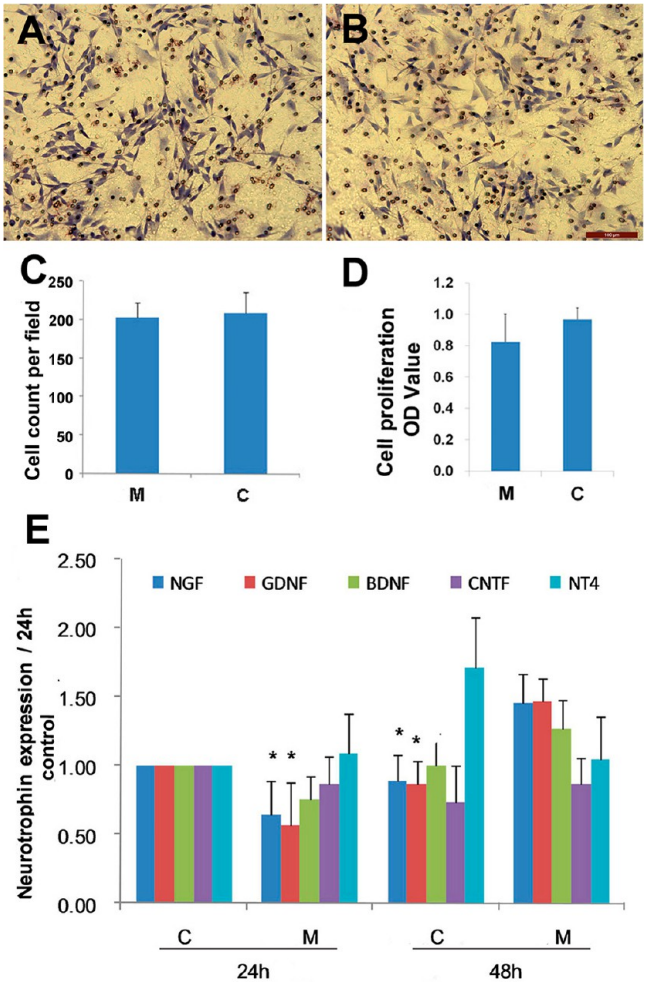

Figure 8. Effect of preconditioned medium on the biological properties of primary cultured Schwann cells. The migration rate of Schwann cells was not significantly affected by the preconditioned medium, as suggested by the transwell analysis (see panels A–C; panel A shows Eosin staining of Schwann cells in the material-preconditioned medium on the bottom of the transwell membrane, whereas panel B shows Eosin staining of Schwann cells in the regular control medium, and panel C shows the Schwann cell count per field). (C, D) Schwann cell proliferation was also not affected by the material preconditioned medium (denoted as M), when compared with that of control (denoted as C), as suggested by the BrdU assay (panel D). (E) Neurotrophin expression in primary Schwann cells 24 and 48 h after incubation with the preconditioned medium did not suggest significant changes, except for an increase in the NGF and GDNF value in the preconditioned medium group by 48 h (asterisk (*) indicates $P < 0.05$, vs 48 h M).

DOI: 10.1021/acsami.5b00215
ACS Appl. Mater. Interfaces 2015, 7, 8437–8450

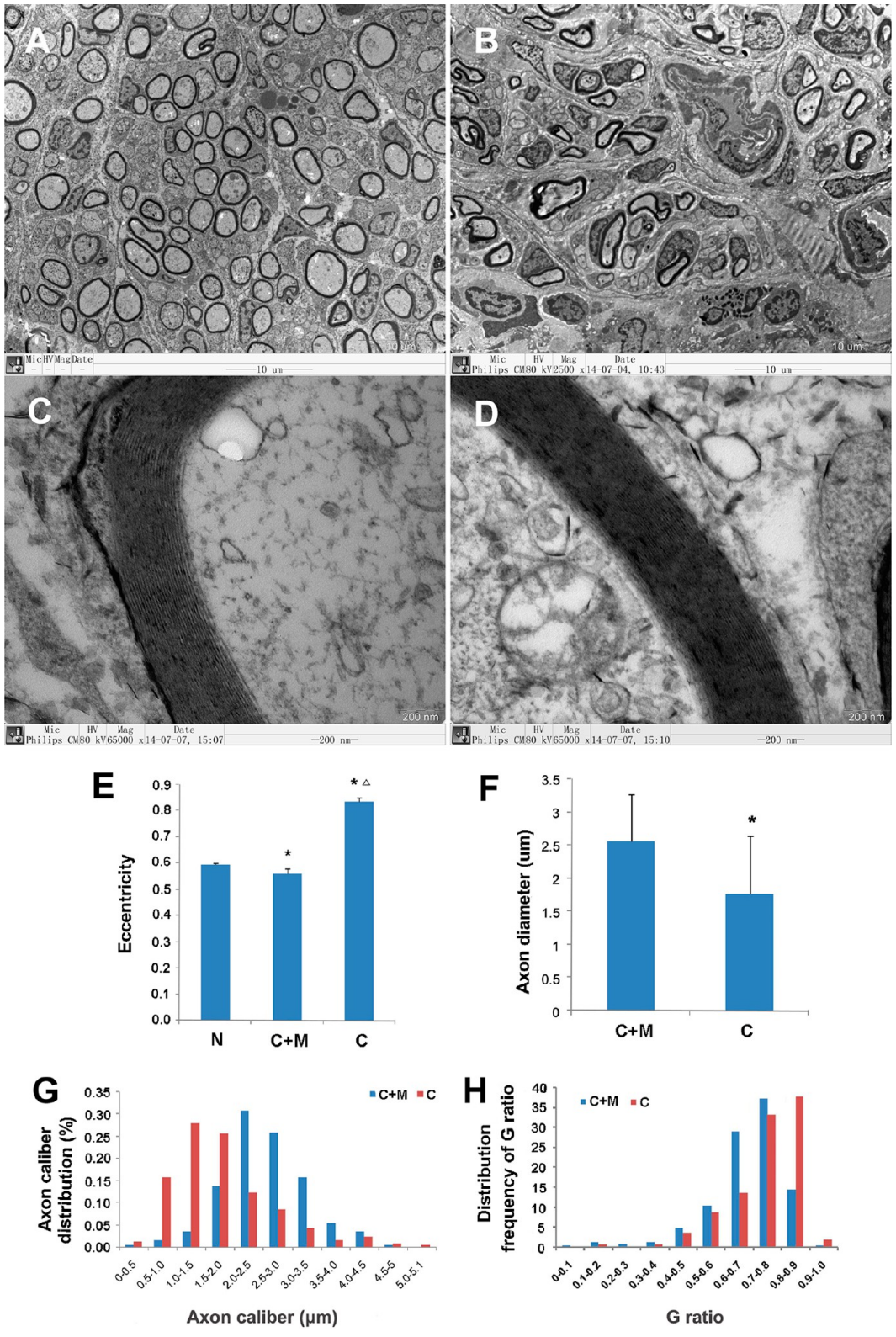

Figure 9. Effect of conduits with an MTAS lining on nerve regeneration. Mature myelin sheath was formed in both the conduit-plus-MTAS group (panels A and C) and the conduit-only group (panels B and D). However, there was a significant difference in the morphology of the regenerated fibers between the two groups. Nerve fibers in the conduit-plus-MTAS group presented a more rounded shape (panel A) with an eccentricity value of 0.56 ± 0.02 (panel E), closer to that of the normal nerve (0.59 ± 0.01). However, the regenerated fibers were significantly smaller than those in the conduit group (0.83 ± 0.02, $P < 0.05$) (panel E), which displayed an oval and longitudinal shape (panel B). In addition, the mean diameter of myelinated fibers in the conduit-plus-MTAS group was significantly larger than that of the conduit-only group (2.56 ± 0.71 μm vs 1.77 ± 0.87 μm, $P < 0.05$ (panel F)). An obvious right shift in the axon diameter and a left shift in the G ratio were noted in the conduit-plus-MTAS group compared with that of the control (C) group (panels G and H). (Legend: C+M = conduit plus MTAS, C = control, asterisk (*) = $P < 0.05$, vs N, and triangle (△) = $P < 0.05$, vs C + M.)

DOI: 10.1021/acsami.5b00215
ACS Appl. Mater. Interfaces 2015, 7, 8437−8450

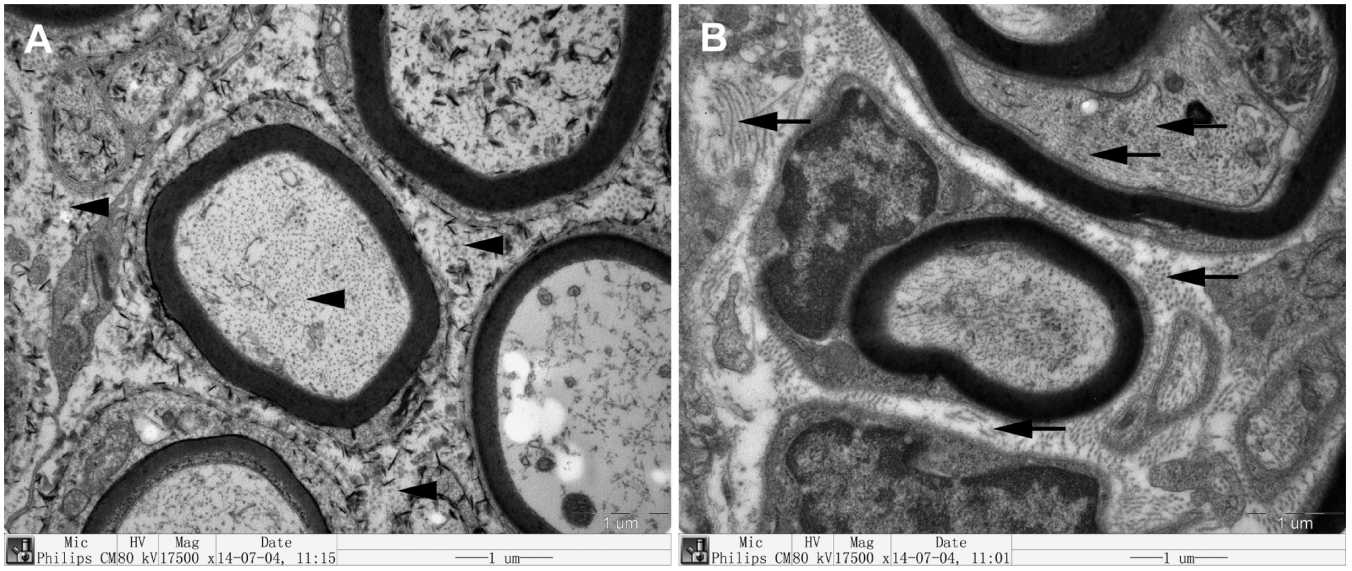

Figure 10. Ultramicroscopic structures of regenerated fibers. Collagen fibers in the extracellular matrix were aligned in concordant directions in nerves repaired with the conduit with an MTAS, as indicated by the evenly scattered dots in panel A (noted by the arrowhead). However, collagen fibers in the extracellular matrix were aligned randomly, as indicated by the coexistence of dots and lines extending in different directions (panel B, denoted by arrows), suggesting the random pattern of neurite projection in the conduit-only group and guided neurite extension in the conduit-plus-MTAS group.

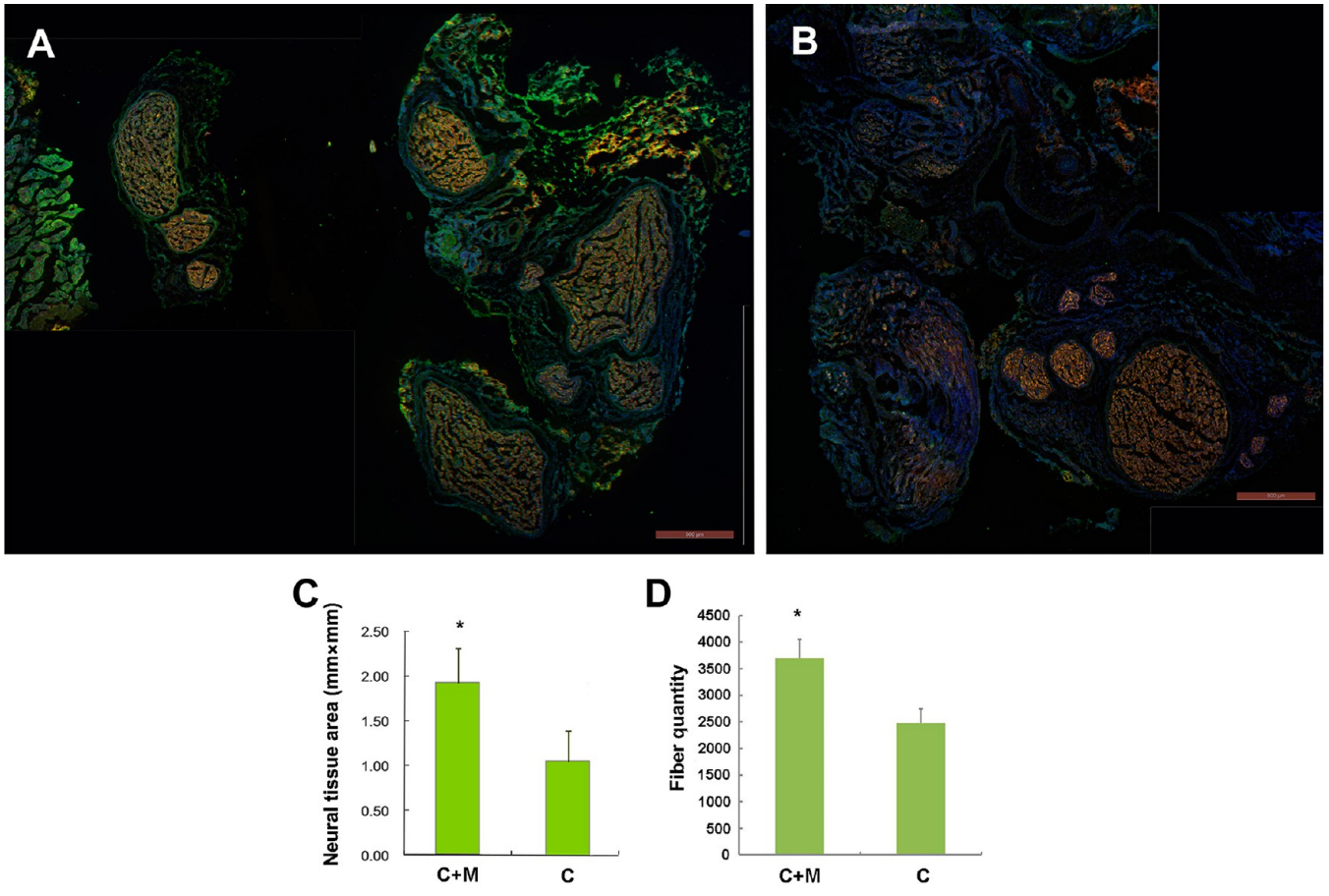

Figure 11. Nerve regeneration at the distal nerve, 5 mm distal from the conduit. Representative transverse sections from (A) the conduit-plus-MTAS group and (B) the conduit-only group. There was a significant increase in the mean total area of neural tissue in the distal nerve repaired with a conduit with an MTAS (C+M) (panel C). The total number of fibers in the distal nerve was significantly higher in rats repaired with conduit with an MTAS (C+M) (panel D). (Asterisk (*) indicates $P < 0.05$, vs control (C).)

DOI: 10.1021/acsami.5b00215
ACS Appl. Mater. Interfaces 2015, 7, 8437−8450

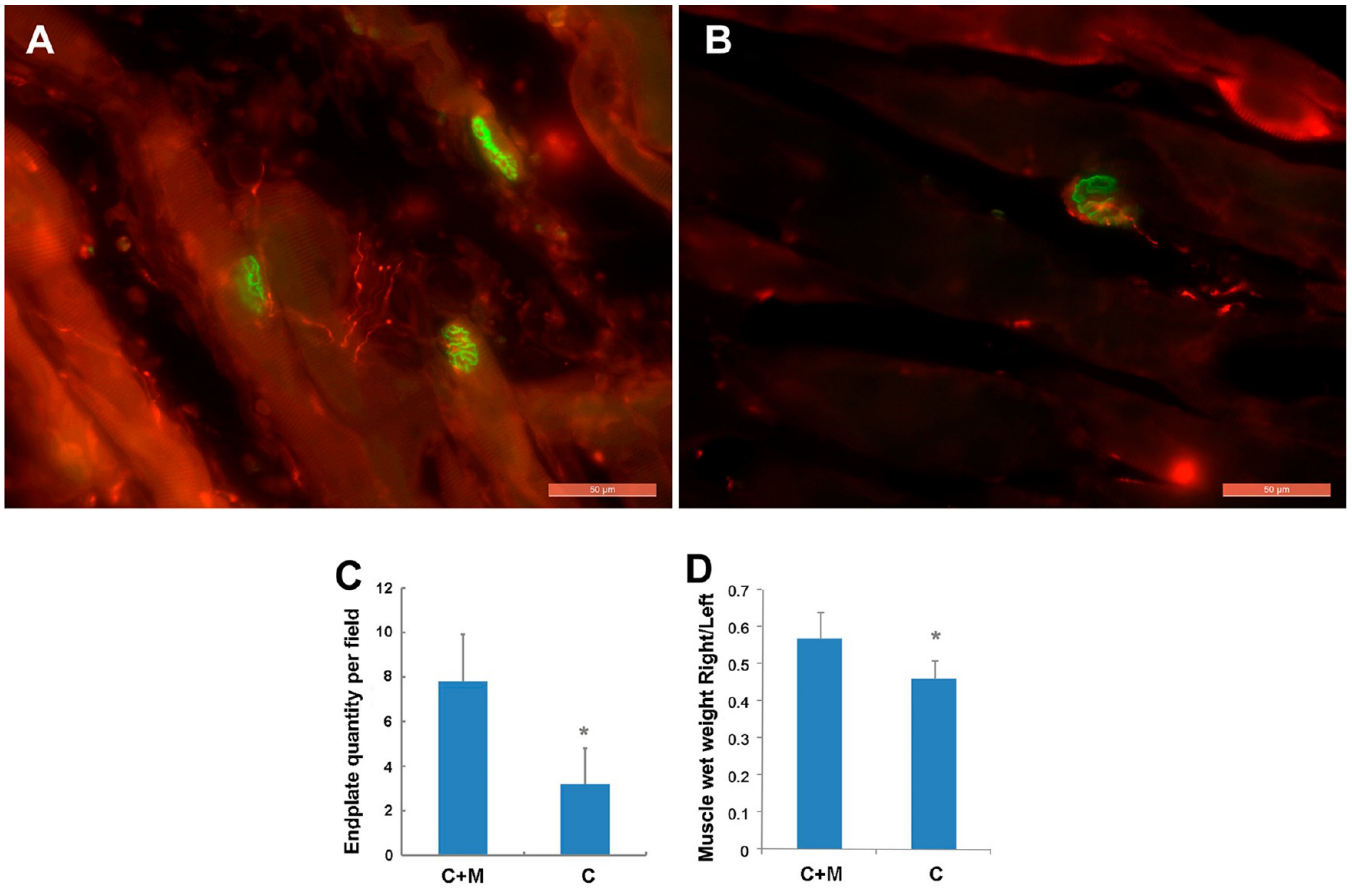

Figure 12. Muscle reinnervation eight weeks after nerve repair. Neuromuscular junctions were formed in both groups. However, the density of the neuromuscular junctions was higher in the conduit-plus-MTAS group (C+M) (panels A and C), compared with the conduit-only group (panels B and C). The muscle wet weight ratio in the conduit-plus-MTAS group was also higher than that of the conduit-only group (panel D). Green indicates Bungarotoxin staining, while red indicates PGP9.5 staining of the nerve terminals. (Asterisk (*) = $P < 0.05$, vs C+M.)

Real-time PCR analysis was applied to assess the capability of Schwann cells to express critical neurotrophic factors when cultured in a preconditioned medium. The expression patterns of BDNF, CNTF, and NT4 remained similar at 24 and 48 h after treatment (Figure 8). Slight but statistically significant increases in NGF and GDNF expression were recorded in the preconditioned medium group at 48 h.

3.5. Effect of Nerve Conduits with MTAS Lining on Sciatic Nerve Regeneration *In Vivo*. We employed 14 mm PLGA nerve conduits with MTAS membranous lining to bridge 10 mm sciatic nerve defects in rats with the aim of determining the efficiency of MTAS for promoting peripheral nerve regeneration *in vivo*. The injured nerve was found to regenerate into the nerve conduit and distal nerve stump by week 8 after repair in both the conduit-only and conduit-plus-MTAS groups (see Figures 9, 10, and 11). No significant differences were evident between the two groups, with regard to the mean area of neural tissue, total number of myelinated fibers, or myelin thickness in the midconduit section. However, the area of neural tissue in the distal nerve stump and the mean quantities of fibers in the conduit-plus-MTAS group were significantly larger than those in the conduit-only group (1.92 ± 0.39 mm^2 vs 1.14 ± 0.34 mm^2, $P < 0.05$; 3698 ± 357 vs 2481 ± 269, $P < 0.05$, Figure 11), suggesting more vigorous regeneration in the former group. In addition, the mean diameter of the myelinated fibers in the conduit-plus-MTAS group was significantly larger than that of the conduit-only group (2.56 ± 0.71 μm vs 1.77 ± 0.87 μm, $P < 0.05$, Figure 10). An obvious right shift in the fiber caliber and a left shift in the G ratio were noted in the conduit-plus-MTAS group, compared with that of the conduit-only group. Myelinated fibers exhibited completely different morphologies in the two groups. Nerve fibers in the conduit-plus-MTAS group presented a more rounded shape with an eccentricity value of 0.56 ± 0.02, closer to that of the normal nerve (0.59 ± 0.01), but the fibers were significantly smaller than those of the conduit group (0.83 ± 0.02, $P < 0.05$), which displayed an oval and longitudinal shape, indicative of two different patterns of nerve growth (see Figures 9 and 10).

To evaluate end organ reinnervation, neuromuscular junction staining was performed. As suggested in Figure 12, double staining of the end-plate and nerve terminals was evident in both groups, suggesting that reinnervation was successful. However, the density of the end-plate in each visual field was significantly higher in the conduit-plus-MTAS group compared with that of the conduit-only group. In addition, the ratio of muscle wet weight on the injury side relative to the contralateral side was significantly larger by month 8 in the conduit-plus-MTAS group than that of the conduit-only group (0.57 ± 0.08 vs 0.46 ± 0.06, $P < 0.05$).

4. DISCUSSION

Despite the greater capability of regeneration, relative to that in the CNS, peripheral nerve regeneration across large nerve defects remains a considerable challenge. Various nerve

DOI: 10.1021/acsami.5b00215
ACS Appl. Mater. Interfaces 2015, 7, 8437−8450

conduits or guides have been developed to bridge this gap to facilitate regeneration;[15−17] however, the outcomes are not clinically satisfactory. After peripheral nerve injury, regenerating axons present a bundle of collaterals to locate the proper pathway and target.[27] The denervated muscle undergoes atrophy with time, and the severity of muscle atrophy is directly related to the length of time it takes for the regenerating nerve to reach the efferent muscle.[28,29] Moreover, the longer the Schwann cells in the distal nerve stump remain denervated, the less likely they are to provide a supportive microenvironment for regenerating nerves.[30,31] Therefore, the regeneration efficiency and speed are essential for effective functional recovery. However, the direction of neurite extension is affected by multiple circumstantial factors, including both chemical and physical cues. Chemical guidance cues involve various neurotrophic factors and should be used on the basis of a thorough understanding of their function, as different combinations of neurotrophic factors are predominant in distinct cellular events, such as proliferation, migration, neurite extension, and myelination.[32,33] Physical cues include material stiffness, roughness, and surface geometry, which are more easily modified for different applications. Recent studies have indicated that micropatterned surfaces are capable of affecting cell morphology and migration[10−14] and are able to induce NSC differentiation and guide the directed growth of neurites from DRG neurons.[34] However, no *in vivo* studies have been documented to date. In the current investigation, we employed a construct with a unique longitudinally aligned and parallel groove topography formed by the assembly of numerous microtubes as the lining of the conduit and tested its potential for promoting peripheral nerve regeneration both *in vitro* and *in vivo*.

Our *in vitro* findings suggested that the parallel and longitudinally aligned groove surface geometry of the MTAS significantly affects the pattern of Schwann cell alignment. In contrast to the typical spiral alignment on the smooth surface of a Petri dish, Schwann cells were aligned in parallel longitudinal lines on the MTAS 24 h after seeding. Schwann cells are essential glial cells in the peripheral nervous system. These cells dedifferentiate to a naive state after peripheral nerve injury and proliferate and migrate to form a band of Büngner that serves as a scaffold for the attachment and extension of regenerating axons.[35] Therefore, the pattern of Schwann cell alignment determines the direction of Schwann cell migration. The guided migration of Schwann cells along the surface topography of the MTAS allows the Schwann cells to bridge the gap in a shorter time and therefore provide a better microenvironment for neurite extension, enabling the nerve to access its target in the most efficient manner. Although studies by Tay et al. revealed that micropatterned surface geometry is able to affect the biological properties and behavior by changing the cell shape,[10] it is not likely that this parallel, longitudinal alignment is caused by alterations in cell morphology, as the width of the Schwann cells is far narrower than that of the groove, and the Schwann cells display an identical bipolar morphology to those grown on a Petri dish. In addition, Schwann cells are polarized and are capable of forming short linear alignments when cultured on smooth Petri dishes by connecting to each other from both ends, although these lines are generally arranged in a spiral manner. Therefore, it is possible that this parallel alignment is the combined result of forced alignment and directed migration in response to local surface geometry cues. We found that as a polarized cell type, Schwann cells are capable of detecting the local geometry and can alter the direction of migration upon encountering obstructions, such as a scratch on the Petri dish surface. The MTAS used in our study constitutes a single-layered assembly of hollow fibrous microtubes with an extremely high degree of fiber alignment.[22,23] The adjacent microtubes form numerous parallel V-shaped grooves with an average width of ∼20 μm, endowing the MTAS with a double-sided surface geometry of parallel and longitudinally aligned grooves. Previous studies have suggested that the width of the grooves, rather than the depth, is a key factor that affects Schwann cell alignment. Moreover, the width of the longitudinal grooves falls in the range of 10−20 μm, which is regarded as optimal for directing Schwann cell alignment and neurite outgrowth.[13]

The peripheral nerve contains mixed fiber components, including sensory fibers protruding from dorsal root ganglion neurons, motor fibers from spinal cord anterior horn motor neurons, and sympathetic fibers from postganglionic sympathetic neurons. Neural cells represent one of the most notable examples of a highly polarized cell type, typically extending one or several neurites to connect to specific targets in the body. These neurons typically extend long processes in multiple directions randomly and synapse with the most adjacent neurons or processes when cultured *in vitro*. However, in the current study, the oriented extension of neurites occurred upon culture on the MTAS, regardless of the neuron type. Therefore, the surface geometry of parallel V-shaped grooves formed by the assembly of microtubes with an extremely high degree of fiber alignment appears to be effective in guiding the oriented migration of Schwann cells and neurite extension from peripheral neurons.

In large nerve defects that require a nerve conduit for repair, the inner surface of the conduit or the inner structures interact directly with the regenerating axons or Schwann cells, acting as a guide for Schwann cell migration and neurite extension. Currently, nerve conduits, either electrospun or fabricated, yield a conduit wall with transversely arranged fibers or interwoven structures.[15,16] Instead of guiding longitudinal migration, these structures may result in a randomized arrangement of Schwann cells and spiraling of regenerating axons, consequently compromising the growth rate and functional recovery. Therefore, we constructed a complex conduit with MTAS as a lining of the inner wall and bridged a 10 mm sciatic nerve defect in rats. Myelinated fibers in the two groups exhibited different morphologies at the transverse midconduit section. The fibers in the conduit with the MTAS were larger in caliber and rounder in shape, as evident from the significantly smaller average eccentricity, whereas the conduit-only group displayed an oval or even bar shape for most myelin fibers, reflecting different patterns of neurite elongation. This difference likely occurred because the surface geometry of the MTAS in the conduit-plus-MTAS group guided orientated growth along the longitudinal grooves on the surface of the construct. As a result, the regenerating fibers grew largely in a straight line and perpendicular to the transverse sections. This finding is consistent with the *in vitro* results of Schwann cell migration and neurite extension on the MTAS. In contrast, more irregularly shaped myelinated fibers were found in the conduit-only group. The oval or irregularly shaped fibers in the conduit group might be a result of the more random growth of regenerating fibers due to the complex surface geometry of the inner conduit wall. Additional evidence supporting this view was found by comparing the alignment of the collagen fibers in

DOI: 10.1021/acsami.5b00215
ACS Appl. Mater. Interfaces 2015, 7, 8437−8450

the extracellular matrix and the neurofilaments in the axons on the transverse sections of EM images. The collagen fibers in the extracellular matrix in the conduit-plus-MTAS group were aligned largely in parallel in the same direction, as suggested by the evenly distributed dots. However, both dots and short lines were found in the conduit-only group, and the lines were arranged in different directions, suggesting a random arrangement of collagen fibers.

In addition, although nerve regeneration and re-establishment of the neuromuscular junction were detected in both groups, the conduits modified with the MTAS lining more effectively supported regeneration than the those without the MTAS lining, as evidenced by the significantly increased quantity of nerve fibers in the distal stump, the greater fiber caliber in the midconduit and the greater muscle wet weight. This improvement might also be a result of oriented nerve guidance, in response to the unique surface geometry of the MTAS, because directed growth of the nerve prevents the nerve fibers from winding through the conduit, in response to a complex surface geometry, and it enables the fibers to reconnect with the target organ more rapidly. This capability is essential for the restoration of muscle function by preventing progressive atrophy due to prolonged denervation. In addition, muscle reinnervation will, in turn, provide more nutrition for nerve fibers. Our *in vivo* results suggest that the MTAS is as effective in guiding oriented growth of regenerating nerve fibers when used as a lining for the conduit as it is *in vitro*.

5. CONCLUSION

A microtube array sheet (MTAS) with a surface geometry of parallel and longitudinally aligned grooves successfully modified the biological behaviors of Schwann cells and peripheral neurons by guiding orientated cell alignment, migration and neurite extension from peripheral neurons *in vitro* without affecting the critical biological activities of the Schwann cells, such as proliferation and neurotrophic factor expression, which are essential for establishing the regeneration microenvironment. When used as the inner lining of a nerve conduit, the MTAS promoted regeneration, as indicated by the larger fiber caliber in the midconduit and greater quantity of fibers in the distal nerve stump. More importantly, the surface geometry guided orientated nerve growth along the MTAS toward the target, an essential requirement for efficient regeneration. Our collective *in vivo* and *in vitro* findings suggest that the novel MTAS is safe and effective in guiding orientated nerve growth without affecting the critical biological properties of Schwann cells.

AUTHOR INFORMATION

Corresponding Authors

*Tel.: +86-21-63089567. E-mail: drliqingfeng@yahoo.cn.
*Tel.: 86-21-63846590*776324. E-mail: Dingwl500@sina.com.

Author Contributions

#These authors contributed equally to this work.

Notes

The authors declare no competing financial interest.

ACKNOWLEDGMENTS

This work is supported by the National Natural Science Funds of China (Project Nos. 31100782, 81271380, 81201505) and by the Natural Science Fund, supported by the Shanghai Committee of Science and Technology (Project Nos. 11ZR1419400 and 1052 nm04200).

ABBREVIATIONS

MTAS, microtube array sheet; DRG, dorsal root ganglion; BDNF, brain-derived neurotrophic factor; CNTF, ciliary neurotrophic factor; GDNF, glial cell line-derived neurotrophic factor; NGF, nerve growth factor; NT4, neurotrophin-4; GAPDH, glyceraldehyde 3-phosphate dehydrogenase

REFERENCES

(1) Best, T. J.; Mackinnon, S. E.; Bain, J. R.; Makino, A.; Evans, P. J. Verification of a free vascularized nerve graft model in the rat with application to the peripheral nerve allograft. *Plast. Reconstr. Surg.* **1993**, *92*, 516−525.

(2) Firat, C.; Geyik, Y.; Aytekin, A. H.; Gul, M.; Kamsl, S.; Yigitcan, B.; Ozcan, C. Comparison of nerve, vessel, and cartilage grafts in promoting peripheral nerve regeneration. *Ann. Plast. Surg.* **2014**, *73*, 54−61.

(3) Yang, X. N.; Jin, Y. Q.; Bi, H.; Wei, W.; Cheng, J.; Liu, Z. Y.; Shen, Z.; Qi, Z. L.; Cao, Y. Peripheral nerve repair with epimysium conduit. *Biomaterials* **2013**, *34*, 5606−5616.

(4) Mohammadi, R.; Vahabzadeh, B.; Amini, K. Sciatic nerve regeneration induced by transplantation of *in vitro* bone marrow stromal cells into an inside-out artery graft in rat. *J. Craniomaxillofac. Surg.* **2014**, *42*, 1389−1396.

(5) Chan, K. M.; Gordon, T.; Zochodne, D. W.; Power, H. A. Improving peripheral nerve regeneration: From molecular mechanisms to potential therapeutic targets. *Exp. Neurol.* **2014**, *261*, 826−835.

(6) Konofaos, P.; Ver Halen, J. P. Nerve repair by means of tubulization: Past, present, future. *J. Reconstr. Microsurg.* **2013**, *29*, 149−164.

(7) Yamanaka, T.; Hosoi, H.; Murai, T.; Kobayashi, T.; Inada, Y.; Nakamura, T. Regeneration of the nerves in the aerial cavity with an artificial nerve conduit—Reconstruction of chorda tympani nerve gaps. *PloS one* **2014**, *9*, No. e92258.

(8) Tang, X.; Xue, C.; Wang, Y.; Ding, F.; Yang, Y.; Gu, X. Bridging peripheral nerve defects with a tissue engineered nerve graft composed of an *in vitro* cultured nerve equivalent and a silk fibroin-based scaffold. *Biomaterials* **2012**, *33*, 3860−3867.

(9) Xu, H.; Holzwarth, J. M.; Yan, Y.; Xu, P.; Zheng, H.; Yin, Y.; Li, S.; Ma, P. X. Conductive PPY/PDLLA conduit for peripheral nerve regeneration. *Biomaterials* **2014**, *35*, 225−235.

(10) Tay, C. Y.; Yu, H.; Pal, M.; Leong, W. S.; Tan, N. S.; Ng, K. W.; Leong, D. T.; Tan, L. P. Micropatterned matrix directs differentiation of human mesenchymal stem cells towards myocardial lineage. *Exp. Cell. Res.* **2010**, *316*, 1159−1168.

(11) Tong, W. Y.; Shen, W.; Yeung, C. W.; Zhao, Y.; Cheng, S. H.; Chu, P. K.; Chan, D.; Chan, G. C.; Cheung, K. M.; Yeung, K. W.; Lam, Y. W. Functional replication of the tendon tissue microenvironment by a bioimprinted substrate and the support of tenocytic differentiation of mesenchymal stem cells. *Biomaterials* **2012**, *33*, 7686−7698.

(12) Beduer, A.; Vieu, C.; Arnauduc, F.; Sol, J. C.; Loubinoux, I.; Vaysse, L. Engineering of adult human neural stem cells differentiation through surface micropatterning. *Biomaterials* **2012**, *33*, 504−514.

(13) Miller, C.; Shanks, H.; Witt, A.; Rutkowski, G.; Mallapragada, S. Oriented Schwann cell growth on micropatterned biodegradable polymer substrates. *Biomaterials* **2001**, *22*, 1263−1269.

(14) Li, G.; Zhao, X.; Zhao, W.; Zhang, L.; Wang, C.; Jiang, M.; Gu, X.; Yang, Y. Porous chitosan scaffolds with surface micropatterning and inner porosity and their effects on Schwann cells. *Biomaterials* **2014**, *35*, 8503−8513.

(15) Yu, W.; Jiang, X.; Cai, M.; Zhao, W.; Ye, D.; Zhou, Y.; Zhu, C.; Zhang, X.; Lu, X.; Zhang, Z. A novel electrospun nerve conduit enhanced by carbon nanotubes for peripheral nerve regeneration. *Nanotechnology* **2014**, *25*, 165102.

DOI: 10.1021/acsami.5b00215
ACS Appl. Mater. Interfaces 2015, 7, 8437−8450

(16) Biazar, E.; Keshel, S. H. Chitosan-cross-linked nanofibrous PHBV nerve guide for rat sciatic nerve regeneration across a defect bridge. *ASAIO J.* **2013**, *59*, 651−659.
(17) Fukuda, Y.; Wang, W.; Ichinose, S.; Katakura, H.; Mukai, T.; Takakuda, K. Laser perforated accordion nerve conduit of poly(lactide-*co*-glycolide-*co*-ε-caprolactone). *J. Biomed. Mater. Res. B: Appl. Biomater.* **2014**, *102*, 674−680.
(18) Patel, S.; Kurpinski, K.; Quigley, R.; Gao, H.; Hsiao, B. S.; Poo, M. M.; Li, S. Bioactive nanofibers: synergistic effects of nano-topography and chemical signaling on cell guidance. *Nano Lett.* **2007**, *7*, 2122−2128.
(19) Huang, N. F.; Patel, S.; Thakar, R. G.; Wu, J.; Hsiao, B. S.; Chu, B.; Lee, R. J.; Li, S. Myotube assembly on nanofibrous and micropatterned polymers. *Nano Lett.* **2006**, *6*, 537−542.
(20) Xu, C. Y.; Inai, R.; Kotaki, M.; Ramakrishna, S. Aligned biodegradable nanofibrous structure: a potential scaffold for blood vessel engineering. *Biomaterials* **2004**, *25*, 877−886.
(21) Ou, K.-L.; Chen, C.-S.; Lin, L.-H.; Lu, J.-C.; Shu, Y.-C.; Tseng, W.-C.; Yang, J.-C.; Lee, S.-Y.; Chen, C.-C. Membranes of epitaxial-like packed, super aligned electrospun micron hollow poly(L-lactic acid) (PLLA) fibers. *Eur. Polym. J.* **2011**, *47*, 882−892.
(22) Yang, J.-C.; Lee, S.-Y.; Tseng, W.-C.; Shu, Y.-C.; Lu, J.-C.; Shie, H.-S.; Chen, C.-C. Formation of Highly Aligned, Single-Layered, Hollow Fibrous Assemblies and the Fabrication of Large Pieces of PLLA Membranes. *Macromol. Mater. Eng.* **2012**, *297*, 115−122.
(23) Shih, Y. H.; Yang, J. C.; Li, S. H.; Yang, W. C. V.; Chen, C. C. Bio-electrospinning of poly(L-lactic acid) hollow fibrous membrane. *Text. Res. J.* **2012**, *82*, 602−612.
(24) Lin, L. C.; Shu, Y. C.; Yang, J. C.; Shie, H. S.; Lee, S. Y.; Chen, C. C. Nano-porous Poly-L-lactic Acid Microtube Array Membranes. *Curr. Nanosci.* **2014**, *10*, 227−234.
(25) Brockes, J. P.; Fryxell, K. J.; Lemke, G. E. Studies on cultured Schwann cells: The induction of myelin synthesis, and the control of their proliferation by a new growth factor. *J. Exp. Biol.* **1981**, *95*, 215−30.
(26) Mantuano, E.; Inoue, G.; Li, X.; Takahashi, K.; Gaultier, A.; Gonias, S. L.; Campana, W. M. The hemopexin domain of matrix metalloproteinase-9 activates cell signaling and promotes migration of schwann cells by binding to low-density lipoprotein receptor-related protein. *J. Neurosci.* **2008**, *28*, 11571−82.
(27) Lago, N.; Rodriguez, F. J.; Guzman, M. S.; Jaramillo, J.; Navarro, X. Effects of motor and sensory nerve transplants on amount and specificity of sciatic nerve regeneration. *J. Neurosci. Res.* **2007**, *85*, 2800−12.
(28) Day, C. S.; Buranapanitkit, B.; Riano, F. A.; Tomaino, M. M.; Somogyi, G.; Sotereanos, D. G.; Kuroda, R.; Huard, J. Insulin growth factor-1 decreases muscle atrophy following denervation. *Microsurgery* **2002**, *22*, 144−151.
(29) Schiaffino, S.; Dyar, K. A.; Ciciliot, S.; Blaauw, B.; Sandri, M. Mechanisms regulating skeletal muscle growth and atrophy. *FEBS J.* **2013**, *280*, 4294−4314.
(30) Huang, J.; Zhang, Y.; Lu, L.; Hu, X.; Luo, Z. Electrical stimulation accelerates nerve regeneration and functional recovery in delayed peripheral nerve injury in rats. *Eur. J. Neurosci.* **2013**, *38*, 3691−3701.
(31) Sulaiman, O. A.; Gordon, T. Role of chronic Schwann cell denervation in poor functional recovery after nerve injuries and experimental strategies to combat it. *Neurosurgery* **2009**, *65*, A105−A114.
(32) Xiao, J.; Kilpatrick, T. J.; Murray, S. S. The role of neurotrophins in the regulation of myelin development. *Neurosignals* **2009**, *17*, 265−276.
(33) Frostick, S. P.; Yin, Q.; Kemp, G. J. Schwann cells, neurotrophic factors, and peripheral nerve regeneration. *Microsurgery* **1998**, *18*, 397−405.
(34) Song, M.; Uhrich, K. E. Optimal micropattern dimensions enhance neurite outgrowth rates, lengths, and orientations. *Ann. Biomed. Eng.* **2007**, *35*, 1812−1820.
(35) Kidd, G. J.; Ohno, N.; Trapp, B. D. Biology of Schwann cells. *Handb. Clin. Neurol.* **2013**, *115*, 55−79.

DOI: 10.1021/acsami.5b00215
ACS Appl. Mater. Interfaces 2015, 7, 8437−8450